# Dynamics and transport properties of Floquet topological edge modes in coupled photonic waveguides

J. Petráček [1,2] and V. Kuzmiak [3]

[1]*Institute of Physical Engineering, Faculty of Mechanical Engineering, Brno University of Technology, Technická 2, 616 69 Brno, Czech Republic*

[2]*Central European Institute of Technology, Brno University of Technology, Purkyňova 656/123, 612 00, Brno, Czech Republic*

[3]*Institute of Photonics and Electronics, Academy of Sciences of the Czech Republic, v.v.i., Chaberská 57, 182 51, Praha 8, Czech Republic*

We study theoretically the Floquet edge states in a photonic analog of the driven Su-Schrieffer-Heeger model implemented by an array of identical single-mode dielectric waveguides, where the time-dependent driving is modeled by periodically bended waveguides. We combine the coupled-mode theory with the Floquet-Bloch analysis and within this framework determine a band structure of the periodic system. We develop a theoretical approach for calculation of the edge states in semi-infinite systems and investigate their topological properties. In particular, we explore the dynamics of the 0- and $\pi$-edge states which reveal profound differences depending on their topological phase. To verify our observations, we simulate the power transport along the end of such a waveguide array and show that its spectra can be assigned to the excitation of the edge modes. The results obtained indicate that driving-induced topological properties of the edge modes can be exploited in controlling flow of light in periodically driven photonic structures and may provide insight into Floquet engineering of the realistic photonic systems.

## I. INTRODUCTION

Topological phases in various dimensions attracted widespread interest since the discovery of the quantum Hall effect [1]. It revealed the existence of a new class of robust quantum phenomena beyond the Landau paradigm of spontaneous symmetry breaking that can be linked to the presence of energy gaps for bulk excitations. It was shown that the topological insulators behave as insulators in the bulk and their properties can have a profound impact on the character of the boundary modes which can propagate along the boundary without backscattering even in the presence of static disorder [2,3]. Discovery of topological insulators has triggered enormous interest in many areas [2] including solid state [4], cold atom [5], and photonic systems [6–10].

A typical example of a one-dimensional topological insulator is the tight-binding Su-Schrieffer-Heeger (SSH) model [11] which describes dimerization in the chain of identical sites coupled via alternating strong and weak bonds. The topological character of the chain is controlled by the relative strength of the intracell and intercell couplings $C_1$ and $C_2$, respectively, and as a consequence of bulk-boundary correspondence principle it supports one topological state localized at each boundary if $|C_1/C_2| < 1$, while its existence is linked to the topological invariant called the Zak phase [12].

Following the development in the field of topological insulators, time-periodic driving was suggested besides a strong magnetic field and spin-orbit coupling as a third alternative that can be used in realizing topologically nontrivial phases. The underlying principle of this area called Floquet engineering [13] is based on the driving of the system with a certain frequency $\Omega$ which leads to a hybridization of the eigenstates of a static system and allows realization of new topologically nontrivial phases that are unaccessible in a static system. The effects of a time-dependent perturbation were employed in ultracold optical lattices [14], time crystals [15], and photonic structures [16,17]. Appropriately selected driving regimes allow for tuning transport regimes from ballistic to localized [18,19] and inducing quantum phase transitions [20]. Periodic driving can change the topological properties of a system. It was shown that in periodically driven systems bulk-edge correspondence has to be generalized and the existence of anomalous edge states (ES) corresponding to unique bulk topological invariants were predicted [21,22]. For example, a system, which is topologically trivial in equilibrium, can become a topological insulator under periodic driving due to breaking of time-reversal symmetry [23]. On the other hand, the time-reversal symmetry breaking is not necessary in driven SSH systems where a gap opening mechanism relies on the spatial periodicity of time-dependent perturbation [24]. Anomalous $\pi$ modes have been recently observed in a photonic Floquet simulator consisting of periodically bended ultrathin metallic arrays of coupled corrugated waveguides, which support spoof surface plasmon polaritons at microwave to infrared frequencies [25]. Unlike the systems subject to periodic driving, any local perturbation in a system with a

nontrivial topology does not lead to change of the topological character of the bulk bands, nevertheless it was shown that local periodic driving can lead to breakdown of the topological protection and dramatic depopulation of the ES [26].

In our paper we study theoretically spectral properties and dynamics of the topologically protected edge states in a photonic Floquet simulator of the driven SSH model. Since in waveguide arrays the propagation distance plays the role of time, the time-dependent perturbations can be realized by the periodically bended waveguides. The substitution is based on exploiting mathematical equivalence between the time-dependent Schrödinger equation and the coupled-mode theory (CMT) and consequently allows for the temporal dynamics of an electronic wave packet to be mapped to spatial evolution of the light field. To calculate the edge states we developed a theoretical approach which yields solutions in semi-infinite structures. We explored the dynamics of the 0- and $\pi$-edge states and we have shown that their properties can be effectively exploited in controlling flow of light.

To fabricate a photonic Floquet simulator several designs may be employed. The first experiments were realized by periodically bending ultrathin metallic arrays of coupled corrugated waveguides, which support spoof surface plasmon polaritons at microwave to infrared range [25,27]. In optical domain, other technologies are available such as a laser-written waveguides in fused silica [28] or dielectric loaded surface plasmon waveguides with in-plane modulation and dielectric waveguide arrays with out-of-plane modulation [26] fabricated by electron beam lithography and direct three-dimensional (3D) laser printing.

The paper is organized as follows: In Sec. II we describe our waveguide array system which mimics the driven SSH model and provides an introduction into the formulation of the CMT based techniques which are described in detail in Appendix. In Sec. III we first present band structures and spectra of the ES which may appear in the gaps, then we describe their properties and demonstrate how they affect the transport properties of the system. We discuss the possibilities of steering of light beam by exploiting topological properties of the ES with respect to both the driving frequency and the phase. In Appendix A 1 we present our implementation of the Floquet-Bloch analysis which extends the method described in Ref. [26] to the case of the global driving and its application for the calculation of a band structure in terms of the quasienergies. The extension of this technique which allows us to calculate the ES in semi-infinite arrays is described in Appendix A 2.

## II. STRUCTURE AND FORMULATION

In this paper we study theoretical characteristics of the topologically protected ES in a photonic Floquet simulator based on one-dimensional (1D) array dielectric coupled waveguides under time-periodic driving. Since in the waveguide model the propagation distance $z$ corresponds to time $t$, the modulation of the coupling coefficients is realized by periodically bending the waveguide in $xz$ plane, see Fig. 1(a). The evolution of the light in the structure is described by CMT
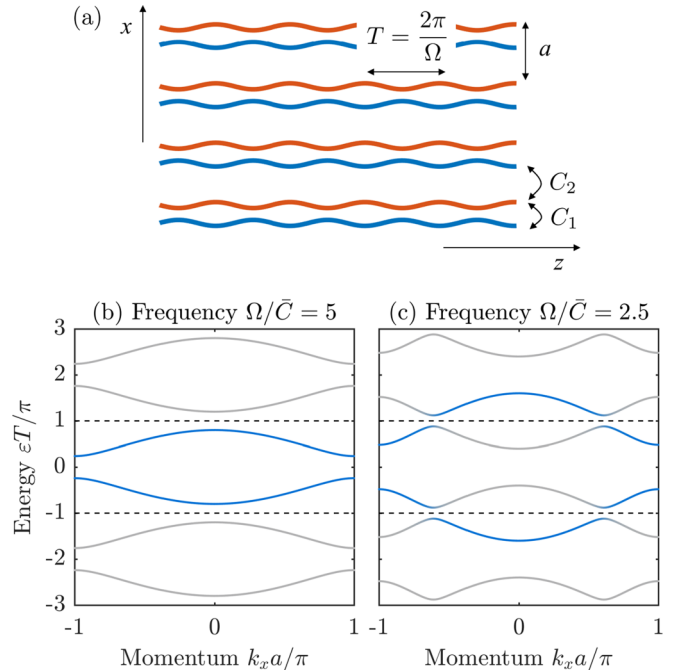


FIG. 1. (a) A schematic picture of the periodically driven waveguide array. The structure consists of two sublattices marked by two different colors with two coupling coefficients $C_1$ and $C_2$. The periods $a$ and $T = 2\pi/\Omega$ in $x$ and $z$ direction, respectively, are indicated. (b) and (c) The band structures for $\Delta C/\bar{C} = \pm 0.3$, $\Delta V/\bar{C} = 0.2$ and (b) $\Omega/\bar{C} = 5$; (c) $\Omega/\bar{C} = 2.5$. The dashed horizontal lines indicate the first Brillouin zone for quasienergy. The color scale represents the spectral weight at a given energy.

[29,30] as

$$i\frac{d\psi_n}{dz} = C_{n-1}\psi_{n-1} + C_n\psi_{n+1},\qquad(1)$$

where $\psi_n$ is the modal amplitude on the $n$th waveguide ($n \in Z$) and $C_n$ is the coupling coefficient between waveguides $n$ and $(n+1)$.

The system is periodic in $x$ direction with the period $a$ that consists of two waveguides so that the coupling coefficients (for fixed $z$) alternate between two values $C_{2m+1} = C_1$ and $C_{2m} = C_2$ where $m \in Z$ and which correspond to the intercell and intracell coupling, respectively. By using the Floquet-Bloch boundary condition

$$\psi_{n+2} = \lambda\psi_n, \quad \lambda \equiv \exp(-ik_x a),\qquad(2)$$

where $k_x$ is the Floquet-Bloch wave number ("momentum") we transform Eq. (1) into the momentum space as

$$i\frac{d}{dz}\begin{pmatrix}\psi_1\\\psi_2\end{pmatrix} = \begin{pmatrix}0 & C_1+C_2\lambda^{-1}\\C_1+C_2\lambda & 0\end{pmatrix}\begin{pmatrix}\psi_1\\\psi_2\end{pmatrix}.\qquad(3)$$

If there is no driving (i.e., $C_{1,2}$ are independent of $z$) the solution has the form $\psi_n(z) \propto \exp(-i\varepsilon z)$, where $\varepsilon$ is referred to as "energy." It is well known that in this static case the SSH model is a band insulator when $|C_1| \neq |C_2|$ with trivial and nontrivial topology when $|C_1| > |C_2|$ and $|C_1| < |C_2|$, respectively. The topological character of the dimerized chain implies a fundamental difference in spectrum of a finite or semi-infinite nontrivial system: A system with nontrivial

topology (unlike the trivial one) supports topologically protected ES exponentially decaying along the $x$ axis and localized near structure ends with an energy $\varepsilon$ inside the gap.

In the following, we consider periodic modulation of coupling coefficients in the form

$$C_{1,2}(z) = \bar{C} \pm \Delta C \pm \Delta V \cos(\Omega z + \varphi), \qquad (4)$$

where $\Delta C$ is the dimerization strength and $\Delta V$ is the driving amplitude. In order to obtain the bulk and edge states we solve Eq. (3) with suitable additional conditions. The procedure is based on the Floquet-Bloch theory [31,32], see also Ref. [26], and is described in more detail in Appendix. Within this formalism a band structure of a system governed by a time-periodic Hamiltonian with period $T = 2\pi/\Omega$ can be unambiguously described in terms of so-called (quasi)energies $\varepsilon$, analogs of the eigenenergies in a time-independent problem. The corresponding Floquet states belong to the extended Hilbert space, which is a direct product of the usual Hilbert space and the space of periodic functions $\exp(ip\Omega t)$, where index $p$ defines a subspace called Floquet replica.

In our paper we assume lossless waveguides, however our method allows us to treat global losses (such as radiation losses due to the bending or ohmic losses) since they are decoupled from dynamics (see, e.g., Ref. [33]) and can be taken into account in the calculation of the transmitted power. We choose such a value of the strength of modulation $\Delta V/\bar{C} = 0.3$ which along the period of the modulation $T$ ensures that one can neglect the losses due to the curvature of the waveguide. Specifically, the upper frequency limit of the driving frequency $\Omega/\bar{C} = 5$ considered in our paper is smaller than those arising from balanced trade-off between the bending losses and the strength of dynamic effects chosen in experimental realizations reported in Refs. [25,26], where $\Omega/\bar{C} \approx 7.5$ and $\Omega/\bar{C} \approx 6.5$, respectively.

## III. RESULTS

### A. Floquet quasienergy spectrum of a driven structure

To demonstrate the properties of quasienergy spectra associated with our system [Fig. 1(a)], we assume two values of dimerization strength $\Delta C = \pm 0.3\bar{C}$, representing the native trivial and nontrivial phase, respectively, and fix the amplitude of the time-dependent modulation at $\Delta V = 0.2\bar{C}$; the values are taken from Ref. [24]. We note that neither the sign of $\Delta C$ nor the modulation shift $\varphi$ in Eq. (4) affects the band structure. However, we will show that $\varphi$ plays an important role in the excitation of the ES which may display strong dependence on the propagation distance. Note that the case $\varphi = \pi$ corresponds to the value assumed in Ref. [24], where nearby bonds have the opposite phases.

The band structures (expressed in normalized quantities) are illustrated in Figs. 1(b) and 1(c) presenting $p = 0, \pm 1$ replicas which are displaced by $p\Omega$. It was shown [24] that one can distinguish two profoundly different regimes: In the high-frequency regime different bands do not overlap at the energy $\varepsilon$ we are interested in, whereas the low-frequency regime occurs when there is more than one state close to $\varepsilon$. If the frequency is high enough the replicas are well separated at any $\varepsilon$ (so we are in the high-frequency regime for any $\varepsilon$) [see Fig. 1(b)] and the bands in the first Brillouin zone
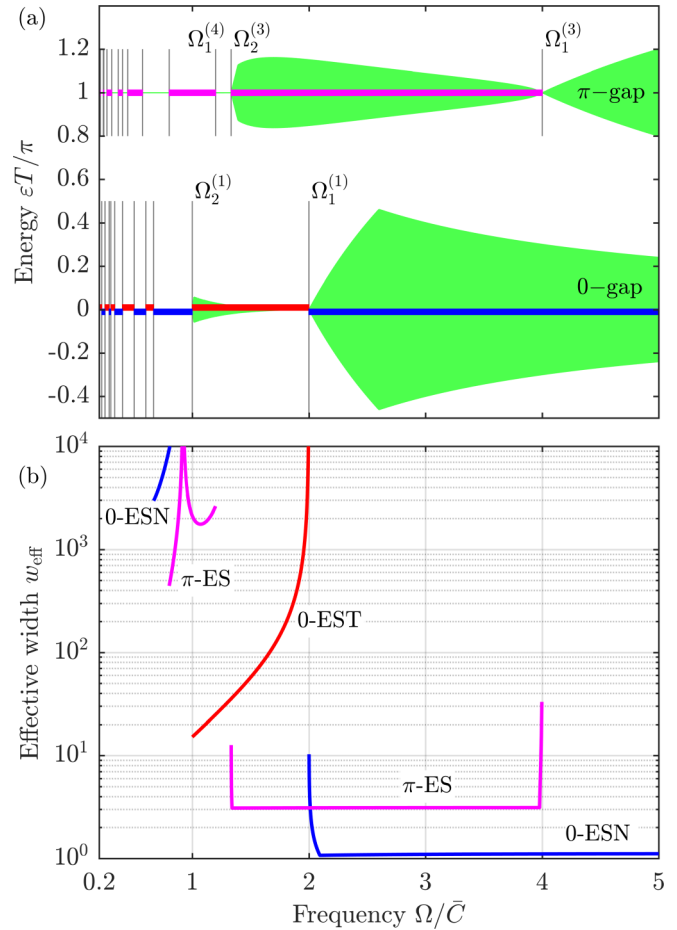


FIG. 2. (a) Maps of the 0 and $\pi$ gaps as a function of the driving frequency $\Omega/\bar{C}$. Thin vertical lines indicate the frequencies at which the gaps are closed. Bold horizontal lines indicate the frequency ranges in which $\pi$-ES (upper panel) and both 0-EST and 0-ESN (lower panel) are supported. EST and ESN denote the ES in the structures in trivial and nontrivial native topological phase, respectively [see also annotation in (b)]. The bold lines corresponding to the 0-EST are slightly vertically shifted with respect to the 0-ESN. (b) Effective width $w_{\mathrm{eff}}$ vs driving frequency $\Omega/\bar{C}$ for the 0- and $\pi$-edge states. Parameters: $\Delta C/\bar{C} = \pm 0.3$ for trivial and nontrivial native topological phase, $\Delta V/\bar{C} = 0.2$.

$-\Omega/2 < \varepsilon \leqslant \Omega/2$ (FBZ) correspond to those of the undriven native structure. In addition to the pre-existent gap centered at zero energy $\varepsilon = 0$ and thus referred to as 0 gap (we consider $\varepsilon$ in FBZ only), the driving induces a new gap centered at $\varepsilon = \Omega/2$ known as $\pi$ gap. The shaded areas in Fig. 2(a) depict the variation of both gaps with the frequency $\Omega/\bar{C}$. By decreasing $\Omega$ one gradually enters the low-frequency regime: the replicas start to overlap with each other and become degenerate at $\varepsilon = \Omega/2$ [see Fig. 1(c)] or $\varepsilon = 0$ and the related gaps are closed. However, due to the presence of driving the corresponding degeneracies are lifted leading to reopening the gaps [24]. The spectra shown in Fig. 1(c) correspond to the case when one is in the low-frequency regime at $\varepsilon = \Omega/2$ while still is in the high-frequency regime at $\varepsilon = 0$. The transition points at which 0 gap closes occur at the frequencies given by $\Omega_m^{(1)} = 2\bar{C}/m$ for $k_x = 0$ and $\Omega_m^{(2)} = 2|\Delta C|/m$ for

$k_x a = \pi$ ($m = 1, 2, \ldots$). The transitions points at which $\pi$ gap closes occur at $\Omega_m^{(3)} = 4\bar{C}/(2m - 1)$ for $k_x = 0$ and at $\Omega_m^{(4)} = 4|\Delta C|/(2m - 1)$ for $k_x a = \pi$. The positions of the transition points are indicated by vertical lines in Fig. 2(a).

### B. Edge states

It is well known that the driven structure can support ES with the quasienergies $\varepsilon = 0$ or $\varepsilon = \Omega/2$ within both 0 or $\pi$ gaps [21,24,34], in the following the states are referred to as 0-ES and $\pi$-ES, respectively. The existence of ES can be verified by evaluating either the band invariant Zak phase [12] or the gap invariants $\nu_0$ and $\nu_\pi$ derived in Ref. [21]. We also calculated the ES directly by solving an eigenvalue problem for a semi-infinite structure (see Appendix A 2). By evaluating the Zak phase we determined the frequency ranges in which the system supports 0- and $\pi$-ES indicated by bold lines in Fig. 2(a). The calculation based on the invariants $\nu_0$ and $\nu_\pi$ provides identical intervals; however, the direct evaluation of the ES yields slightly different results in the range $\Omega/\bar{C} < 0.8$. The origin of these discrepancies was attributed to the numerical instabilities in searching eigensolutions of Eq. (A12) for which $|\lambda_\alpha| < 1$ in the case $|\lambda_\alpha| \approx 1$, which is typical at such low frequencies.

The features shown in Fig. 2(a) resemble those found for quantum systems in Refs. [21,24,34]. Namely, we confirmed that in the high-frequency limit the behavior of the driven system corresponds to that of the undriven one so that the 0 gap hosts the ES when the static system is in nontrivial phase. In contrast, the presence of the ES in the $\pi$ gap is independent of the native topology of an undriven system.

We characterize a spatial extent of the ES with the effective width defined as $w_{\text{eff}} = \log(0.5)/\log(\lambda_{\max})$, where $\lambda_{\max} \equiv \max |\lambda_\alpha|$ is the maximum value occurring in the expansion Eq. (A10), i.e., $w_{\text{eff}}$ estimates the distance (expressed in the waveguide number) at which the intensity of ES drops to half of its initial value. The results shown in Fig. 2(b) demonstrate a surprising fact that the most of the ES are significantly delocalized—see the ranges $\Omega/\bar{C} < 1$ for 0-ES and $\Omega/\bar{C} < 4/3$ for $\pi$-ES, where the $w_{\text{eff}}$ mostly exceeds $10^4$, and as a result they cannot be effectively excited by a finite source. We observe strong localization only for 0-ES in the frequency range $\Omega/\bar{C} > 2$ (system in nontrivial native phase) where $w_{\text{eff}} \sim 1$ and for $\pi$-ES in the interval $4/3 < \Omega/\bar{C} < 4$ for both native phases where $w_{\text{eff}} \sim 3$. The effective width obtained for the 0-ES in trivial phase in the frequency range $1 < \Omega/\bar{C} < 2$ indicates a substantionally weaker localization only when $\Omega/\bar{C} \to 1$, while it predicts an extendedlike wave function pattern as the $w_{\text{eff}}$ grows rapidly when $\Omega/\bar{C} \to 2$. Figure 2(b) also illustrates that $w_{\text{eff}}$ associated with $\pi$-ES does not depend on the native topological phase. It is important to keep in mind that the $w_{\text{eff}}$ is by its definition independent of the propagation distance $z$ and, therefore, it is of interest to analyze the dynamics of the corresponding wave functions.

The properties of the effective width shown in Fig. 2(b) unveil a profoundly different behavior between the 0-ES which occur in the high-frequency range when $\Omega/\bar{C} > 2$ for the system in nontrivial native phase and those which appear in the 0 gap for trivial native phase when $1 < \Omega/\bar{C} < 2$. In order to gain a deeper insight into the latter observation,
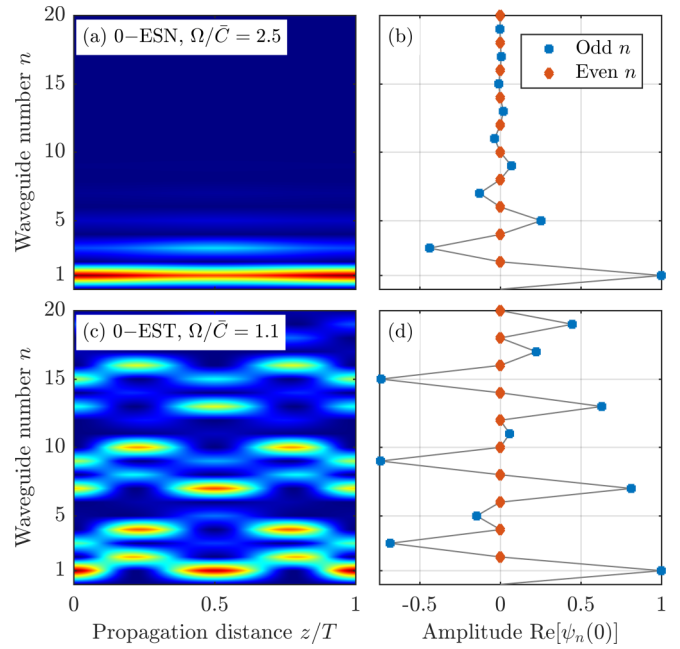


FIG. 3. Zero edge states in the semi-infinite structure. The left panels [(a) and (c)]: Intensity distributions $|\psi_n(z)|^2$ over one period for $\Omega = 2.5$ and $\Omega = 1.1$, respectively. The right panels [(b) and (d)]: The corresponding eigenfunctions at the beginning of the period $\psi_n(0)$, the colors of the markers correspond to those assigned to sublattices shown in Fig. 1(a). For calculation of $\psi_n(z)$ we set $\varphi = 0$, other parameters are the same as in Fig. 2.

we present in Figs. 3(a) and 3(b) and Figs. 3(c) and 3(d) the distributions of the intensity and the real part of the eigenfunction (at $z = 0$) belonging to the 0-ES at $\Omega/\bar{C} = 2.5$ and $\Omega/\bar{C} = 1.1$, respectively. The patterns obtained for $\Omega/\bar{C} = 2.5$ resemble to a great extent those describing ES of undriven structures in nontrivial phase: the wave function $\psi_n(0)$ is nonzero only on "odd" sublattice ($n = 1, 3, 5, \ldots$). Its intensity distribution $|\psi_n(z)|^2$ exhibits weak dependence on the normalized propagation distance $z/T$ and $\psi_n(z)$ converges to the wave function associated with the ES of the undriven structure when $\Omega/\bar{C}$ is further increased. The nature of 0-ES at $\Omega/\bar{C} = 1.1$ state [Figs. 3(c)-3(d)] essentially differs from that corresponding to the high-frequency regime as its wave function reveals a delocalized pattern: the wave function for $z = 0$ and $z = T/2$ is nonzero on an odd sublattice only and its strong variation along the propagation distance corresponds to excitation of $p = \pm 1$ replicas and leads to periodic exchange of the intensity between an odd and even ($n = 2, 4, 6, \ldots$) sublattice.

We have verified that the $\pi$-ES for both native phases appear in the same frequency ranges [see Fig. 2(a)] and they possess the same effective width. Let us now focus on the dynamical properties of the $\pi$-ES. To do so we display in Fig. 4 the states at $\Omega/\bar{C} = 2.5$ and $\Omega/\bar{C} = 1.6$ (only nontrivial phase). The intensity profiles of the $\pi$-ES at $\Omega/\bar{C} = 2.5$ for both native phases are localized on an even sublattice at $z = 0$ (or $z = T$) and display a periodic dependence of the spatial distribution on the propagation distance, which shows a remarkable difference. Namely, the intensity distribution for the trivial phase $z = T/2$ occupies mostly waveguide $n = 1$
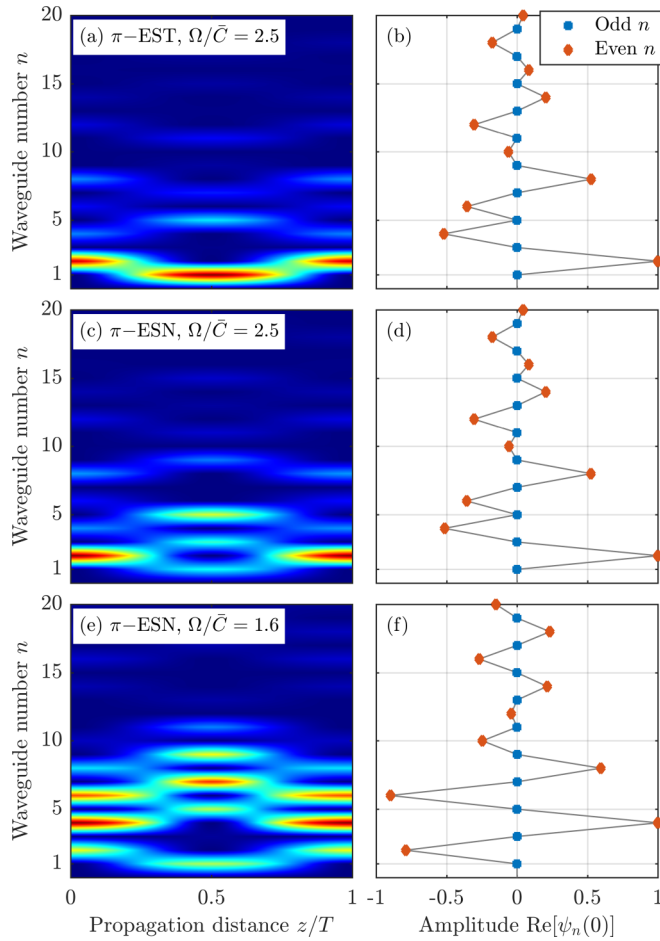
FIG. 4. $\pi$-edge states in the semi-infinite structure. Description of the graphs and the other parameters are the same as in Fig. 3.

[Figs. 4(a) and 4(b)], while the wave function for the nontrivial phase is shifted to higher $n$ waveguides inside the structure [Figs. 4(c) and 4(d)] and this effect is significantly enhanced as the modulation frequency is decreased to $\Omega/\bar{C} = 1.6$ [Fig. 4(e)]. Both periodically varying patterns reflect the excitation of the $p = 0$ and $p = 1$ Floquet replicas at a given driving frequency and give rise to periodic exchange of the intensity between odd and even sublattice.

The results shown in Figs. 3 and 4 illustrate behavior of the wave function pattern at certain frequencies. Since these distributions may significantly change with the frequency as well as within one period $T$, we evaluate another quantity which we call the center of the ES $n_0(z) = \sum_n n|\psi_n(z)|^2/\sum_n |\psi_n(z)|^2$. The results of the numerical calculation for several values of the propagation distance are presented in Fig. 5, where we used $1 \leqslant n \leqslant 200$. The spectral dependencies reveal qualitatively different behavior between the 0- [Figs. 5(a) and 5(b)] and $\pi$-ES [Fig. 5(c)] in a given topological phase. In the high-frequency limit the 0-ES should always converge to the ES supported by the undriven structure for which the center of ES is given by formula $n_0^{(\text{native})} = (1 + \eta^2)/(1 - \eta^2)$ with $\eta = (\bar{C} - \Delta C)/(\bar{C} + \Delta C)$; indeed Fig. 5(a) demonstrates that $n_0 \to n_0^{(\text{native})} = 1.817$ as $\Omega/\bar{C} \to \infty$ irrespective to the propagation distance $z$. On the other hand, $n_0(z)$ for the same ES exhibits an enhanced dependence on the $z$ as $\Omega/\bar{C}$ decreases
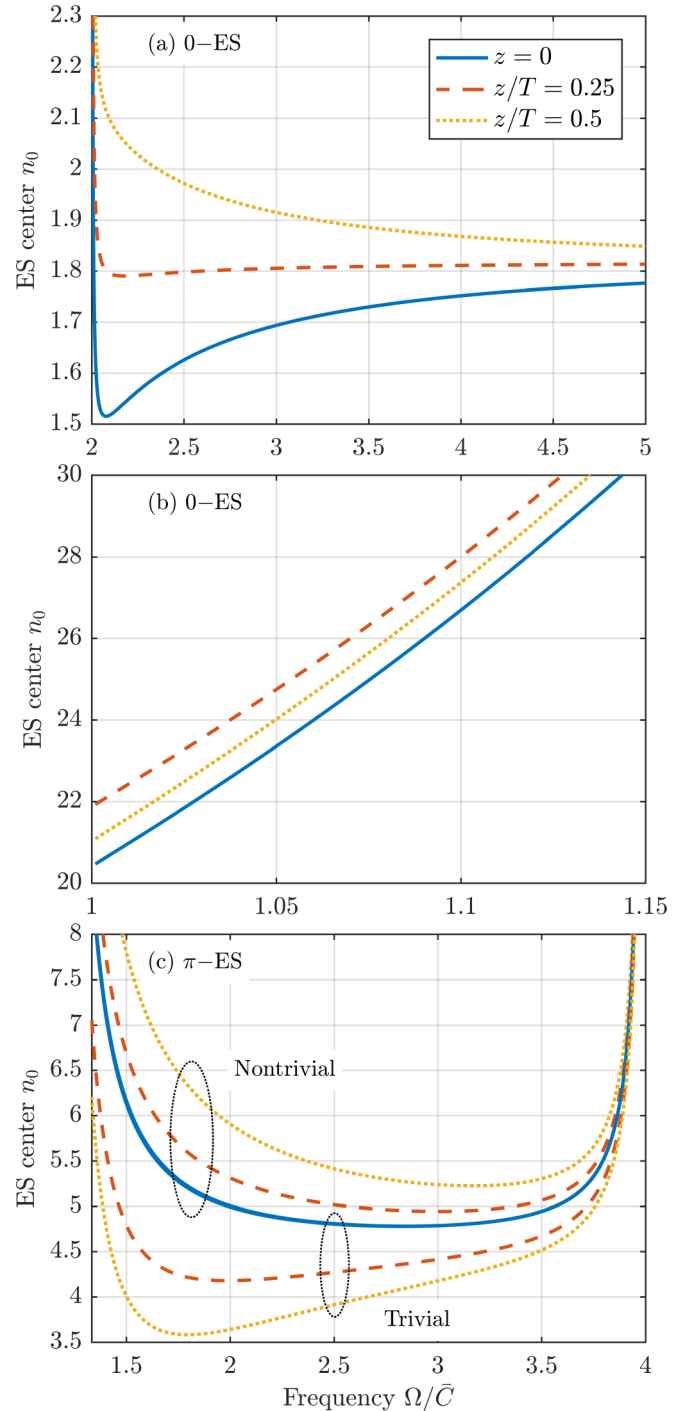


FIG. 5. The ES center $n_0$ for 0- and $\pi$-ES (see descriptions in the graphs) at several positions $z$ [see the legend in (a)]. Other parameters are the same as in Fig. 3.

[Fig. 5(a)] and becomes divergent as $\Omega/\bar{C} \to 2+$. We note that such unbounded behavior is not observed for the $n_0(z)$ associated with 0-ES [Fig. 5(b)] when $\Omega/\bar{C} \to 1+$. In this case $n_0(z)$ grows monotonically in the range $1 < \Omega/\bar{C} < 2$ and shows unbounded behavior as $\Omega/\bar{C} \to 2-$. By inspecting the dependence of the $n_0(z)$ associated with the $\pi$-ES we found that $n_0$ at $z = 0$ is independent of the native topological phase—see the blue curve in Fig. 5(c). This invariance breaks

down as $z$ increases in the first half of the period ($0 \leqslant z \leqslant T/2$), where $n_0(z)$ is shifted towards the waveguides with smaller and larger waveguide number $n$ for the trivial and nontrivial phase, respectively. The $n_0(z)$ for both $\pi$-ES in the range $1.5 \lesssim \Omega/\bar{C} \lesssim 3.5$ was found to yield the values indicating fairly localized wave functions, while $n_0(z)$ becomes unbounded as $\Omega/\bar{C}$ approaches the transition points at both ends of the relevant spectral region. We note that the features described above play key role in the interpretation of the transport properties of the system which are presented in the following subsection.

## C. Transport properties

To verify the properties of the ES described in the previous section and to demonstrate their possible role in controlling flow of light in driven systems we simulate the power transport along the edge of such a structure. The waveguide array is excited at $z = 0$ in the edge waveguide $n = 1$, i.e., $\psi_n(0) = \delta_{1n}$, and the evolution of the field $\psi_n(z)$ in the structure with length $L = 200/\bar{C}$ is calculated by solving numerically Eq. (1) by using the Runge-Kutta technique. We note that this approach can be employed in calculation of the realistic waveguide arrays when the coupling coefficients and other relevant parameters such as ohmic and bending induced losses (all obtained numerically, e.g., from Comsol) are implemented. A semi-infinite system is modeled with a sufficiently large finite structure, for the given $L$ we assumed an array with 200 waveguides. First, we present the results expressed in terms of the relative power $P_{ES} = \sum_{n=1}^{25} |\psi_n(L)|^2$ transmitted to the output of the structure. Naturally, for a sufficiently long structure the $P_{ES}$ does not contain diffracted power (associated with the excitation of bulk modes spreading ballistically) and in fact it represents a fraction of input power coupled into the ES. In Fig. 6 we show the relative power $P_{ES}$ as the function of driving frequency $\Omega$ for structures with both native topological phases and for several phase shifts $\varphi$. The curves correspond to different transport regimes that can be controlled by varying the driving frequency $\Omega$ and the phase $\varphi$. The features observed can be assigned to the excitation of relevant ES that may lead to major suppression of the diffraction. Some of the regimes are illustrated in Figs. 7(a)–7(d).

Specifically, for the trivial native phase, the high transmission in the range $4/3 < \Omega/\bar{C} < 4$ shown in Fig. 6(a) for $\varphi \neq 0$ is due to the excitation of $\pi$-ES in this frequency range [Fig. 2(a)] while for $\Omega/\bar{C} > 4$ there are no ES available and as a result transmitted power is zero. The evolution of the field intensity in the zero transmission regime where the whole input signal is diffracted is shown in Fig. 7(a). In the range $4/3 < \Omega/\bar{C} < 4$, $P_{ES}$ exhibits a strong dependence on $\varphi$ following typical behavior of both $\pi$-ES shown in Fig. 4. For example, when $\varphi = 0$, the $\pi$-ES exhibit zero field at odd sublattice at the beginning of the structure $z = 0$, they cannot be excited with field intensity localized solely on the waveguide $n = 1$, and, consequently, $P_{ES} = 0$. A nonzero value of $\varphi$ means that the ES considered is shifted within the period $T$ and thus it may be excited with a modified efficiency. In the case of the $\pi$-ES presented in Fig. 4(a), increasing $\varphi$ in the interval $0 < \varphi < \pi$ gives rise to growing intensity on the
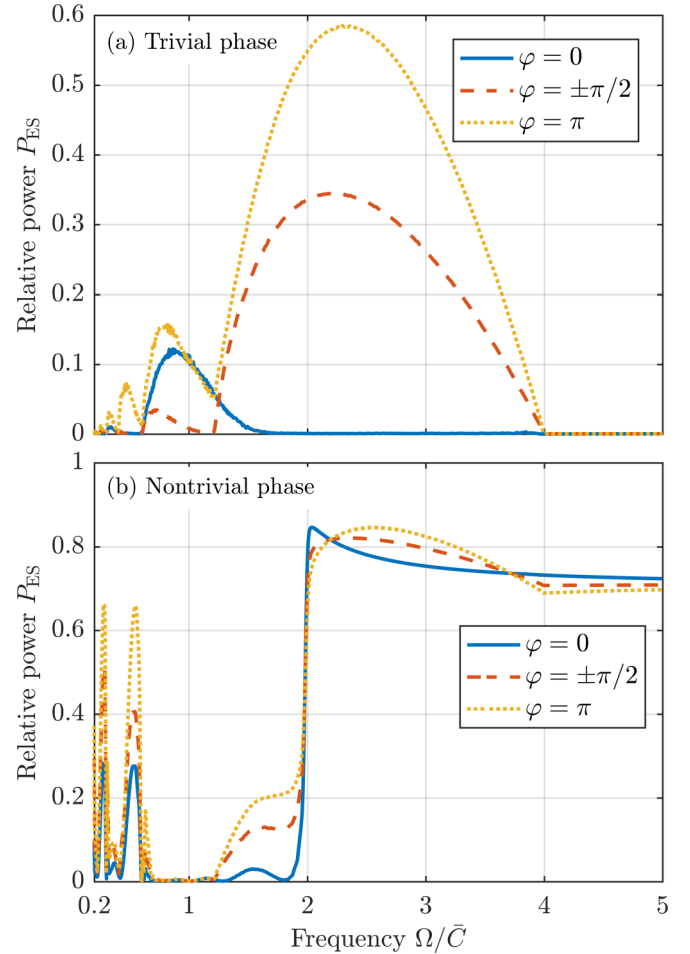


FIG. 6. The relative transmitted power $P_{ES}$ vs driving frequency $\Omega$ evaluated for four phase shifts $\varphi$ of the modulation (see the legend) in structures with length $L = 200/\bar{C}$, excited in waveguide $n = 1$, $\psi_n(0) = \delta_{1n}$, and for (a) trivial and (b) nontrivial phase. The results for $\varphi = \pm\pi/2$ cannot be distinguished in the scale of the graph. Other parameters are the same as in Fig. 2.

waveguide $n = 1$ which in turn leads to increasing excitation efficiency and thus results into the gradual enhancement of the $P_{ES}$ observed in Fig. 6(a), with maximum $P_{ES}$ at $\varphi = \pi$. The corresponding intensity evolution for $\Omega/\bar{C} = 2.5$ and $\varphi = \pi$, where $P_{ES}$ has its maximum with respect to both parameters, is presented in Fig. 7(c).

We have shown that in the frequency range $1 < \Omega/\bar{C} < 2$ there exist besides $\pi$-ES also 0-ES [Fig. 2(a)]. However, they do not affect the power spectrum in Fig. 6(a) in the range $1.6 \lesssim \Omega/\bar{C} < 2$ since they cannot be effectively excited by a signal in one waveguide due to the large effective width [see Fig. 2(b)]. When the modulation frequency is decreased in the range $1 < \Omega/\bar{C} \lesssim 1.6$, the effective width decreases and the amplitude arising from the 0-ES becomes significant; the effect clearly manifests itself in nonzero transmission for $\varphi = 0$. Furthermore, considering only the interval $1 \lesssim \Omega/\bar{C} \lesssim 1.2$, for $\varphi = 0$ and $\varphi = \pi$ the 0-ES are excited approximately with the same efficiency so the related power dependencies are nearly the same. In contrast, for $\varphi = \pm\pi/2$ the 0-ES are weakly excited [their intensity $|\psi_1(\pm T/4)|^2$ is small yet
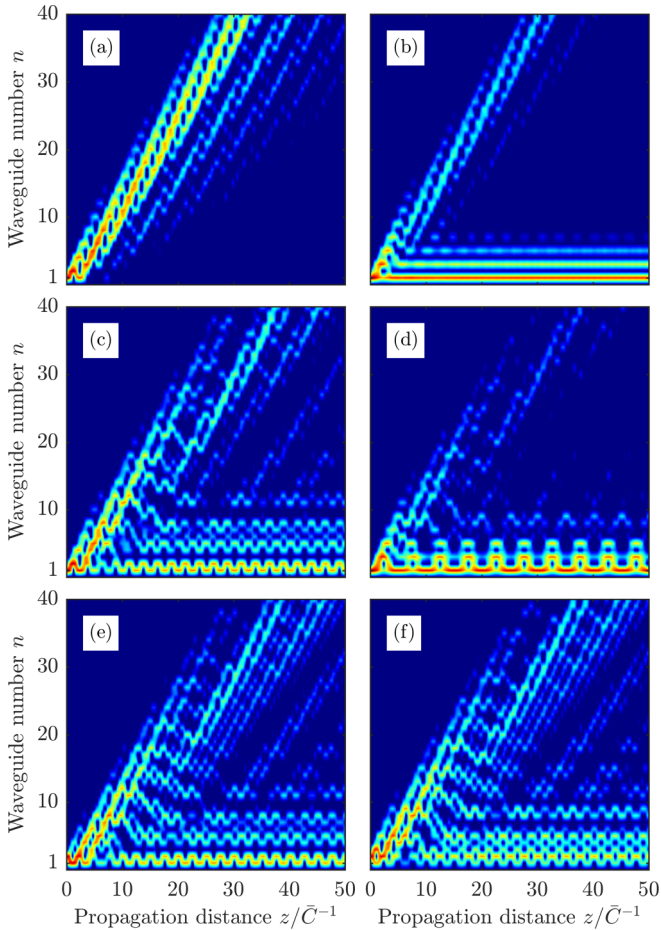
FIG. 7. The evolution of the field intensity $|\psi_n(z)|^2$ in structures as in Fig. 6 in the following cases: (a)–(d) Waveguide $n = 1$ excited, $\psi_n(0) = \delta_{1n}$; (e) and (f) waveguide $n = 2$ excited, $\psi_n(0) = \delta_{2n}$. (a), (c), and (e) Trivial phase; (b), (d), and (f) nontrivial phase. (a) and (b) $\Omega/\bar{C} = 5$; (c)–(f) $\Omega/\bar{C} = 2.5$. (a), (b), (e), and (f) $\varphi = 0$; (c) and (d) $\varphi = \pi$. In order to provide more instructive maps we used a logarithmic color scale and set its minimum at 0.01.

nonzero], which results in almost zero transmission. Such a behavior is in agreement with the properties of the 0-ES demonstrated in Figs. 3(c) and 3(d) for $\Omega/\bar{C} = 1.1$.

Considering the nontrivial native phase [see Fig. 6(b)] the spectra are dominated by excitation of the strongly localized 0-ES in the frequency range $\Omega/\bar{C} > 2$ superimposed with a minor component associated with the excitation of the $\pi$-ES when $\varphi \neq 0$ in the interval $4/3 < \Omega/\bar{C} < 4$. An exclusive excitation of the 0-ES, which is illustrated in Fig. 7(b), exhibits a weak dependence on the phase $\varphi$ [see the $P_{\mathrm{ES}}$ in the range $\Omega/\bar{C} > 4$ in Fig. 6(b)], which becomes negligible in the high-frequency limit. The excitation of $\pi$-ES in the range $4/3 < \Omega/\bar{C} < 2$ affects the spectra in Fig. 6(b) similarly as in Fig. 6(a) except its contribution to the total power is weaker. It complies with the observation that field intensity at $z = T/2$ on the waveguide $n = 1$ associated with the $\pi$-ES for nontrivial phase is smaller than that of the trivial phase [see Figs. 4(a) and 4(c)]. Therefore, $\pi$-ES excitation efficiency is lower in the case of the nontrivial native phase. A simultaneous excitation of the 0- and $\pi$-ES when $\varphi = \pi$

is demonstrated in Fig. 7(d), here the intensity exhibits an oscillatory behavior due to the interference between these two states.

We have seen that by setting the phase $\varphi$ one can selectively excite various ES and, in this way, control the transport properties of the structure. The intensity patterns shown in Figs. 3 and 4 suggest that the same effect may be achieved by choosing a suitable combination of the incident waves. For example, for the trivial native phase and frequencies $4/3 < \Omega/\bar{C} < 4$, $\pi$-ES is excited with highest efficiency when the signal is applied to the waveguide $n = 1$ and the phase $\varphi = \pi$ [Fig. 7(c)], or, alternatively, when the signal is applied to the waveguide $n = 2$ and the phase $\varphi = 0$ [Fig. 7(e)]. For the nontrivial native phase and frequencies $2 < \Omega/\bar{C} < 4$, only $\pi$-ES can be excited when the signal is applied to the waveguide $n = 2$ and $\varphi = 0$ [Fig. 7(f)].

We note that the spectra in Fig. 6 display additional features that cannot be explained with excitation of the ES. Specifically, all the peaks in the frequency range $\Omega/\bar{C} < 1$ [Figs. 6(a) and 6(b)] and the peak at $\Omega/\bar{C} = 1.54$ for the nontrivial phase and $\varphi = 0$ [Fig. 6(b)] are attributed to the resonances in the bulk spectra. The effect was confirmed by calculating the dependence of the $P_{\mathrm{ES}}$ on structure length $L$ which shows decreasing dependence for the mentioned features, in contrast to those associated with the excitation of the ES which are not affected when the length is changed.

## IV. CONCLUSION

We study spectral properties and dynamics of the Floquet edge states in an array of dielectric waveguides with periodical modulation of coupling which mimics a driven Su-Schrieffer-Heeger model. The system is described by means of the coupled mode theory and the resulting equations are solved by the Floquet-Bloch analysis. Within this framework we developed an approach for calculation of edge states of semi-infinite systems and explored their topological properties.

In particular, we describe in detail spectral properties and dynamics of the 0- and $\pi$-edge states and we have shown that they reveal profoundly different behavior depending on the topological phase. In order to gain an additional insight into quasienergy spectra we determined a spatial extent of the edge states characterized by an effective width and we identified the relevant frequency ranges in which edge states can be excited by a finite source. We found that both 0-ES and $\pi$-ES for $\Omega/\bar{C} < 1$ are significantly delocalized and thus cannot be used for guiding light along structure edges. In the case of the nontrivial native phase the 0-ES is strongly localized only in the high-frequency range $\Omega/\bar{C} > 2$, where the state resembles the behavior of the edge state of the undriven structure, i.e., it exhibits a moderate dependence on the propagation distance and occupies mainly the odd sublattice. In contrast, the 0-ES which for the system in the trivial native phase exists in the frequency range $1 < \Omega/\bar{C} < 2$, shows a substantially weaker localization. The $\pi$-ES for both native phases are well localized only in the range $4/3 < \Omega/\bar{C} < 4$ with the same effective width at $z = 0$; however, their wave functions display a topology-sensitive dynamics which reflects the excitation of

the relevant Floquet replicas ($p = 0$ and $p = 1$) and leads to periodic exchange of the intensity between the odd and even sublattice. The features observed determine the excitation efficiency of the ES and crucially affect the transport properties of the system.

To verify the results of the Floquet-Bloch analysis we simulated power transport along the edge of the coupled system for various parameters and identified different transport regimes. We found that the excitation of the ES may lead to major suppression of the diffraction when $\Omega/\bar{C} > 1$. Namely, for the nontrivial native phase, the most dominant effect is the high transmission in the range $\Omega/\bar{C} > 2$ due to the excitation of the 0-ES, while for the trivial native phase, the nonzero transmission in the range $4/3 < \Omega/\bar{C} < 4$ is associated with excitation of the $\pi$-ES. We also demonstrated that the dependence of the excitation efficiency on the driving phase and the shape of the input signal can be conveniently exploited for selective excitation of various ES.

In summary, we have proved that our CMT-based approach represents an efficient tool in the analysis of the impact of driving on a 1D topological insulator given by the photonic realization of the SSH model. The results obtained suggest that the topological ideas can be employed in controlling localization and steering of light in a periodically driven waveguide array and may provide an insight into the physics of the realistic photonic systems under periodic driving.

## APPENDIX

### 1. Floquet-Bloch analysis, bulk states

The coupled mode equations [Eq. (1) or (3)] have the form of the time-dependent Schrödinger equation

$$i\frac{\partial|\psi(t)\rangle}{\partial t} = H(t)|\psi(t)\rangle \tag{A1}$$

(we use $t$ rather than $z$ and set $\hbar = 1$, hereafter) with time-periodic Hamiltonian $H(t + T) = H(t)$, $T = 2\pi/\Omega$. The Floquet-Bloch theorem states that there is a complete set of solutions of the form

$$|\psi_\alpha(t)\rangle = \exp(-i\varepsilon_\alpha t)|u_\alpha(t)\rangle, \tag{A2}$$

where $|u_\alpha(t)\rangle = |u_\alpha(t + T)\rangle$, $\varepsilon_\alpha$ is called quasienergy, and the subscript $\alpha$ labels different solutions. Substitution of Eq. (A2) into Eq. (A1) leads to the equation analogous to the time-independent Schrödinger equation

$$\left[H(t) - i\frac{\partial}{\partial t}\right]|u_\alpha(t)\rangle = \varepsilon_\alpha|u_\alpha(t)\rangle, \tag{A3}$$

where the operator on the left-hand side is called the Floquet Hamiltonian with $|u_\alpha(t)\rangle$ being its eigenstates. Now

we expand $H(t)$ and $|u_\alpha(t)\rangle$ in Eq. (A3) into Fourier series

$$H(t) = \sum_{p=-\infty}^{\infty} H_p \exp(-ip\Omega t), \tag{A4}$$

$$|u_\alpha(t)\rangle = \sum_{p=-\infty}^{\infty} |u_{\alpha,p}\rangle \exp(-ip\Omega t), \tag{A5}$$

and obtain set of equations which leads to solving of the eigenproblem

$$\sum_{q=-\infty}^{\infty} (H_{p-q} - p\delta_{pq}\Omega)|u_{\alpha,q}\rangle = \varepsilon_\alpha|u_{\alpha,q}\rangle. \tag{A6}$$

Within our model, the Hamiltonian is defined on the right-hand side of Eq. (3) together with Eq. (4) in which we assume $\varphi = 0$. By using the definitions $C_{1,2}^{(0)} = \bar{C} \pm \Delta C$ one obtains

$$H_0 = \begin{pmatrix} 0 & C_1^{(0)} + C_2^{(0)}\lambda^{-1} \\ C_1^{(0)} + C_2^{(0)}\lambda & 0 \end{pmatrix}, \tag{A7}$$

$$H_1 = H_{-1} = \frac{\Delta V}{2}\begin{pmatrix} 0 & 1 - \lambda^{-1} \\ 1 - \lambda & 0 \end{pmatrix}, \tag{A8}$$

and $H_p = 0$ for $p \neq 0, \pm 1$. Thus Eq. (A6) can be simplified as

$$(H_0 - p\Omega)|u_{\alpha,p}\rangle + H_1(|u_{\alpha,p-1}\rangle + |u_{\alpha,p+1}\rangle) = \varepsilon_\alpha|u_{\alpha,p}\rangle. \tag{A9}$$

In order to solve the eigenproblem given by Eq. (A9) the Fourier series have to be truncated. Here we used the condition $|p| \leqslant 4\bar{C}/\Omega$ assuring that all replicas with quasienergies within the first Brillouin zone are taken into account; moreover, we numerically verified stability of this criterion.

The bulk modes are solutions of Eq. (A9) for $|\lambda| = 1$, i.e., $\pi < k_x a \leqslant \pi$.

### 2. Edge states (ES)

While solutions of Eq. (A9) with $|\lambda| \neq 1$ cannot occur in the infinite structure, the ES in finite or semi-infinite structures can be formed by their suitable superposition in the form

$$|\psi(t)\rangle = \sum_\alpha Q_\alpha|\psi_\alpha(t)\rangle, \tag{A10}$$

where $Q_\alpha$ are expansion coefficients, provided (i) $\varepsilon$ is constant (therefore, we drop the subscript $\alpha$ of the $\varepsilon$ hereafter), (ii) the superposition decays into the structure, and (iii) fulfils boundary condition(s) at the structure end(s). As a result, the subscript $\alpha$ acquires a different meaning as it labels all the solutions of Eq. (A9) with given energy $\varepsilon$ for all possible values $\lambda_\alpha$. In this paper we consider ES at the boundary of the semi-infinite structure defined with $n = 1, 2, 3, \ldots$ in Eq. (1). Thus conditions (ii) and (iii) translate to $|\lambda_\alpha| < 1$ and $\psi_0(z) = 0$, respectively. Note that the superposition describes the field in one period in $x$ direction only. In order to obtain the complete profile we have to use Eq. (2), i.e., to multiply $|\psi_\alpha(t)\rangle$ in Eq. (A10) with appropriate power of $\lambda_\alpha$. If we denote $|u_{\alpha,p}\rangle = (A_{\alpha,p} \ B_{\alpha,p})^T$ and use Eqs. (2) and (A10), condition (iii) takes the form

$$\sum_\alpha (B_{\alpha p}/\lambda_\alpha)Q_\alpha = 0. \tag{A11}$$

This is a set of homogeneous equations for unknown $Q_\alpha$, its nonzero solution indicates an existence of ES. In our computer program the problem was solved with the singular value decomposition.

Because $\varepsilon$ is constant, it is advantageous to rewrite Eq. (A9) into a form suitable for calculation of $\lambda_\alpha$ for a given value of $\varepsilon$. To this aim we substitute Eqs. (A7) and (A8) into Eq. (A9), multiply the result from the left by matrix

$$\begin{pmatrix} \lambda_\alpha & 0 \\ 0 & 1 \end{pmatrix},$$

and group the terms that contain $\lambda_\alpha$. After a few straightforward steps we obtain the generalized eigenproblem

$$X_p|u_{\alpha,p}\rangle + W(|u_{\alpha,p-1}\rangle + |u_{\alpha,p+1}\rangle)$$
$$= \lambda_\alpha[Y_p|u_{\alpha,p}\rangle + W(|u_{\alpha,p-1}\rangle + |u_{\alpha,p+1}\rangle)]. \quad \text{(A12)}$$

where

$$X_p = \begin{pmatrix} 0 & C_2^{(0)} \\ C_1^{(0)} & -\varepsilon - p\Omega \end{pmatrix}, \quad \text{(A13)}$$

$$Y_p = \begin{pmatrix} \varepsilon + p\Omega & -C_1^{(0)} \\ -C_2^{(0)} & 0 \end{pmatrix}, \quad \text{(A14)}$$

$$W = \frac{\Delta V}{2}\begin{pmatrix} 0 & -1 \\ 1 & 0 \end{pmatrix}. \quad \text{(A15)}$$

Thus the main steps for obtaining ES are as follows:

(1) Define $\Omega$ and $\varepsilon$.

(2) Solve Eq. (A12) for $\lambda_\alpha$, $|u_{\alpha,p}\rangle$; take all solutions for which $|\lambda_\alpha| < 1$.

(3) Solve Eq. (A11) for $Q_\alpha$, a nonzero solution indicates an existing ES.

(4) Possibly use Eq. (A10) for a calculation of the wave function of the ES.

[1] K. von Klitzing, G. Dorda, and M. Pepper, Phys. Rev. Lett. **45**, 494 (1980).

[2] M. Z. Hasan and C. L. Kane, Rev. Mod. Phys. **82**, 3045 (2010).

[3] J. E. Moore, Nature (London) **464**, 194 (2010).

[4] T. Zhang et al., Phys. Rev. Lett. **103**, 266803 (2009).

[5] M. Leder et al., Nat. Commun. **7**, 13112 (2016).

[6] A. B. Khanikaev and G. Shvets, Nat. Photon. **11**, 763 (2011).

[7] C. M. Rechtsmann et al., Nature (London) **496**, 196 (2013).

[8] G. Q. Liang and Y. D. Chong, Phys. Rev. Lett. **110**, 203904 (2013).

[9] L. Lu, J. D. Joannopoulos, and M. Soljacic, Nat. Photon. **8**, 821 (2017).

[10] T. Ozawa et al., Rev. Mod. Phys. **91**, 015006 (2019).

[11] W. P. Su, J. R. Schrieffer, and A. J. Heeger, Phys. Rev. Lett. **42**, 1698 (1979).

[12] J. Zak, Phys. Rev. Lett. **62**, 2747 (1989).

[13] T. Oka and S. Kitamura, Ann. Rev. Condens. Matter Phys. **10**, 387 (2019).

[14] A. Eckardt and E. Anisimovas, New J. Phys. **17**, 093039 (2015).

[15] F. Wilczek, Phys. Rev. Lett. **109**, 160401 (2012).

[16] I. L. Garanovich, S. Longhi, A. A. Sukhorukov, and Y. S. Kivshar, Phys. Rep. **518**, 1 (2012).

[17] S. Longhi and K. Staliunas, Opt. Commun. **281**, 4343 (2008).

[18] S. Longhi, M. Marangoni, M. Lobino, R. Ramponi, P. Laporta, E. Cianci, and V. Foglietti, Phys. Rev. Lett. **96**, 243901 (2006).

[19] H. Li, T. Kottos, and B. Shapiro, Phys. Rev. A **97**, 023846 (2018).

[20] F. Cardano et al., Nat. Commun. **7**, 11439 (2016).

[21] J. K. Asboth, B. Tarasinski, and P. Delplace, Phys. Rev. B **90**, 125143 (2014).

[22] M. S. Rudner, N. H. Lindner, E. Berg, and M. Levin, Phys. Rev. X **3**, 031005 (2013).

[23] T. Oka and H. Aoki, Phys. Rev. B **79**, 081406(R) (2009).

[24] V. Dal Lago, M. Atala, and L. E. F. Foa Torres, Phys. Rev. A **92**, 023624 (2015).

[25] Q. Cheng et al., Phys. Rev. Lett. **122**, 173901 (2019).

[26] Z. Fedorova (Cherpakova) et al., Light: Sci. Appl. **8**, 63 (2019).

[27] Q. Cheng et al., arXiv:1810.00054.

[28] M. Bellec, C. Michel, H. Zhang, S. Tzortzakis, and P. Delplace, Europhys. Lett. **119**, 14003 (2017).

[29] X. Shi, X. Chen, B. A. Malomed, N. C. Panoiu, and F. Ye, Phys. Rev. B **89**, 195428 (2014).

[30] A. Hardy and W. Streifer, J. Light. Technol. **3**, 1135 (1985).

[31] J. H. Shirley, Phys. Rev. **138**, B979 (1965).

[32] H. Sambe, Phys. Rev. A **7**, 2203 (1973).

[33] J. Petráček and V. Kuzmiak, Phys. Rev. A **98**, 023806 (2018).

[34] M. Fruchart, Phys. Rev. B **93**, 115429 (2016).